Approaching the motional ground state of a 10 kg object

Chris Whittle,[1] Evan D. Hall,[1] Sheila Dwyer,[2] Nergis Mavalvala,[1] Vivishek Sudhir,[1,3] R. Abbott,[4] A. Ananyeva,[4] C. Austin,[5] L. Barsotti,[1] J. Betzwieser,[6] C. D. Blair,[6,7] A. F. Brooks,[4] D. D. Brown,[8] A. Buikema,[1] C. Cahillane,[4] J. C. Driggers,[2] A. Effler,[6] A. Fernandez-Galiana,[1] P. Fritschel,[1] V. V. Frolov,[6] T. Hardwick,[5] M. Kasprzack,[4] K. Kawabe,[2] N. Kijbunchoo,[9] J. S. Kissel,[2] G. L. Mansell,[2,1] F. Matichard,[4,1] L. McCuller,[1] T. McRae,[9] A. Mullavey,[6] A. Pele,[6] R. M. S. Schofield,[10] D. Sigg,[2] M. Tse,[1] G. Vajente,[4] D. C. Vander-Hyde,[11] Hang Yu,[1] Haocun Yu,[1] C. Adams,[6] R. X. Adhikari,[4] S. Appert,[4] K. Arai,[4] J. S. Areeda,[12] Y. Asali,[13] S. M. Aston,[6] A. M. Baer,[14] M. Ball,[10] S. W. Ballmer,[11] S. Banagiri,[15] D. Barker,[16] J. Bartlett,[16] B. K. Berger,[17] D. Bhattacharjee,[18] G. Billingsley,[4] S. Biscans,[19,4] R. M. Blair,[16] N. Bode,[20,21] P. Booker,[20,21] R. Bork,[4] A. Bramley,[6] K. C. Cannon,[22] X. Chen,[7] A. A. Ciobanu,[8] F. Clara,[16] C. M. Compton,[16] S. J. Cooper,[23] K. R. Corley,[13] S. T. Countryman,[13] P. B. Covas,[24] D. C. Coyne,[4] L. E. H. Datrier,[25] D. Davis,[11] C. Di Fronzo,[23] K. L. Dooley,[26,27] P. Dupej,[25] T. Etzel,[4] M. Evans,[19] T. M. Evans,[6] J. Feicht,[4] P. Fulda,[28] M. Fyffe,[6] J. A. Giaime,[5,6] K. D. Giardina,[6] P. Godwin,[29] E. Goetz,[5,18,30] S. Gras,[19] C. Gray,[16] R. Gray,[25] A. C. Green,[28] E. K. Gustafson,[4] R. Gustafson,[31] J. Hanks,[16] J. Hanson,[6] R. K. Hasskew,[6] M. C. Heintze,[6] A. F. Helmling-Cornell,[10] N. A. Holland,[9] J. D. Jones,[16] S. Kandhasamy,[32] S. Karki,[10] P. J. King,[16] Rahul Kumar,[16] M. Landry,[16] B. B. Lane,[19] B. Lantz,[17] M. Laxen,[6] Y. K. Lecoeuche,[16] J. Leviton,[31] J. Liu,[20,21] M. Lormand,[6] A. P. Lundgren,[33] R. Macas,[26] M. MacInnis,[19] D. M. Macleod,[26] S. Márka,[13] Z. Márka,[13] D. V. Martynov,[23] K. Mason,[19] T. J. Massinger,[19] R. McCarthy,[16] D. E. McClelland,[9] S. McCormick,[6] J. McIver,[4,30] G. Mendell,[16] K. Merfeld,[10] E. L. Merilh,[16] F. Meylahn,[20,21] T. Mistry,[34] R. Mittleman,[19] G. Moreno,[16] C. M. Mow-Lowry,[23] S. Mozzon,[33] T. J. N. Nelson,[6] P. Nguyen,[10] L. K. Nuttall,[33] J. Oberling,[16] Richard J. Oram,[6] C. Osthelder,[4] D. J. Ottaway,[8] H. Overmier,[6] J. R. Palamos,[10] W. Parker,[6,35] E. Payne,[36] R. Penhorwood,[31] C. J. Perez,[16] M. Pirello,[16] H. Radkins,[16] K. E. Ramirez,[37] J. W. Richardson,[4] K. Riles,[31] N. A. Robertson,[4,25] J. G. Rollins,[4] C. L. Romel,[16] J. H. Romie,[6] M. P. Ross,[38] K. Ryan,[16] T. Sadecki,[16] E. J. Sanchez,[4] L. E. Sanchez,[4] T. R. Saravanan,[32] R. L. Savage,[16] D. Schaetzl,[4] R. Schnabel,[39] E. Schwartz,[6] D. Sellers,[6] T. Shaffer,[16] B. J. J. Slagmolen,[9] J. R. Smith,[12] S. Soni,[5] B. Sorazu,[25] A. P. Spencer,[25] K. A. Strain,[25] L. Sun,[4] M. J. Szczepańczyk,[28] M. Thomas,[6] P. Thomas,[16] K. A. Thorne,[6] K. Toland,[25] C. I. Torrie,[4] G. Traylor,[6] A. L. Urban,[5] G. Valdes,[5] P. J. Veitch,[8] K. Venkateswara,[38] G. Venugopalan,[4] A. D. Viets,[40] T. Vo,[11] C. Vorvick,[16] M. Wade,[41] R. L. Ward,[9] J. Warner,[16] B. Weaver,[16] R. Weiss,[19] B. Willke,[21,20] C. C. Wipf,[4] L. Xiao,[4] H. Yamamoto,[4] L. Zhang,[4] M. E. Zucker,[19,4] and J. Zweizig[4]

[1]*LIGO, Massachusetts Institute of Technology, Cambridge, MA 02139, USA*
[2]*LIGO Hanford Observatory, Richland, WA 99352, USA*
[3]*Department of Mechanical Engineering, Massachusetts Institute of Technology, Cambridge, MA 02139**
[4]*LIGO, California Institute of Technology, Pasadena, CA 91125, USA*
[5]*Louisiana State University, Baton Rouge, LA 70803, USA*
[6]*LIGO Livingston Observatory, Livingston, LA 70754, USA*
[7]*OzGrav, University of Western Australia, Crawley, Western Australia 6009, Australia*
[8]*OzGrav, University of Adelaide, Adelaide, South Australia 5005, Australia*
[9]*OzGrav, Australian National University, Canberra, Australian Capital Territory 0200, Australia*
[10]*University of Oregon, Eugene, OR 97403, USA*
[11]*Syracuse University, Syracuse, NY 13244, USA*
[12]*California State University Fullerton, Fullerton, CA 92831, USA*
[13]*Columbia University, New York, NY 10027, USA*
[14]*Christopher Newport University, Newport News, VA 23606, USA*
[15]*University of Minnesota, Minneapolis, MN 55455, USA*
[16]*LIGO Hanford Observatory, Richland, WA 99352, USA*
[17]*Stanford University, Stanford, CA 94305, USA*
[18]*Missouri University of Science and Technology, Rolla, MO 65409, USA*
[19]*LIGO, Massachusetts Institute of Technology, Cambridge, MA 02139, USA*
[20]*Max Planck Institute for Gravitational Physics (Albert Einstein Institute), D-30167 Hannover, Germany*
[21]*Leibniz Universität Hannover, D-30167 Hannover, Germany*
[22]*RESCEU, University of Tokyo, Tokyo, 113-0033, Japan.*
[23]*University of Birmingham, Birmingham B15 2TT, UK*
[24]*Universitat de les Illes Balears, IAC3—IEEC, E-07122 Palma de Mallorca, Spain*
[25]*SUPA, University of Glasgow, Glasgow G12 8QQ, UK*
[26]*Cardiff University, Cardiff CF24 3AA, UK*
[27]*The University of Mississippi, University, MS 38677, USA*
[28]*University of Florida, Gainesville, FL 32611, USA*
[29]*The Pennsylvania State University, University Park, PA 16802, USA*

[30] University of British Columbia, Vancouver, BC V6T 1Z4, Canada
[31] University of Michigan, Ann Arbor, MI 48109, USA
[32] Inter-University Centre for Astronomy and Astrophysics, Pune 411007, India
[33] University of Portsmouth, Portsmouth, PO1 3FX, UK
[34] The University of Sheffield, Sheffield S10 2TN, UK
[35] Southern University and A&M College, Baton Rouge, LA 70813, USA
[36] OzGrav, School of Physics & Astronomy, Monash University, Clayton 3800, Victoria, Australia
[37] The University of Texas Rio Grande Valley, Brownsville, TX 78520, USA
[38] University of Washington, Seattle, WA 98195, USA
[39] Universität Hamburg, D-22761 Hamburg, Germany
[40] Concordia University Wisconsin, 2800 N Lake Shore Dr, Mequon, WI 53097, USA
[41] Kenyon College, Gambier, OH 43022, USA

The motion of a mechanical object — even a human-sized object — should be governed by the rules of quantum mechanics. Coaxing them into a quantum state is, however, difficult: the thermal environment masks any quantum signature of the object's motion. Indeed, the thermal environment also masks effects of proposed modifications of quantum mechanics at large mass scales. We prepare the center-of-mass motion of a 10 kg mechanical oscillator in a state with an average phonon occupation of 10.8. The reduction in temperature, from room temperature to 77 nK, is commensurate with an 11 orders-of-magnitude suppression of quantum back-action by feedback — and a 13 orders-of-magnitude increase in the mass of an object prepared close to its motional ground state. This begets the possibility of probing gravity on massive quantum systems.

The apparent classical behavior of tangibly massive objects is, according to conventional quantum mechanics, the symptom of decoherence. Thermal decoherence, caused by the interaction of a system with a thermal environment, is by far the most pervasive. For a mechanical oscillator of mass m and natural frequency Ω_0, thermal decoherence induces motion characterized by spectral density $S_x^{\text{th}}[\Omega_0] = (2n_{\text{th}}[\Omega_0] + 1)S_x^{\text{zp}}[\Omega_0]$, where $n_{\text{th}}[\Omega_0] \approx k_B T/\hbar\Omega_0$ is the average thermal phonon occupation due to the environment (at temperature T) and $S_x^{\text{zp}}[\Omega_0] = 8x_{\text{zp}}^2/\Gamma_0[\Omega_0]$ is its motional zero-point fluctuation, $x_{\text{zp}} = \sqrt{\hbar/(2m\Omega_0)}$, concentrated in a frequency band of width $\Gamma_0[\Omega_0]$. Thermal fluctuations obscure signatures of decoherence that allegedly arise from modifications of quantum mechanics at large masses [1–4], and limit the sensitivity of mechanical transducers in metrology applications [5]. Techniques to probe both frontiers call for large mass mechanical objects prepared in pure quantum states.

Over the past decade, progressively larger objects all the way to nanomechanical oscillators have been prepared in their motional ground state [6–10]. A vast majority of these experiments rely on isolating the oscillator in an elastic or electromagnetic trap in the $\gtrsim 100$ kHz frequency range, embedded in a sideband-resolved electromagnetic cavity, typically in a cryogenic environment. These methods do not address a number of technical challenges unique to mechanical oscillators above the milli-/gram mass scale. For one, the large optical power required to trap massive oscillators introduces extraneous heating and other opto-mechanical nonlinearities. Meanwhile, the low resonant frequency of large suspended oscillators doubly compounds the problem of thermal decoherence by in-creasing the intrinsic thermal motion ($n_{\text{tot}} \propto 1/\Omega_0$) and precluding efficient cavity sideband cooling. Therefore a different route is needed to prepare large-mass oscillators in pure quantum states.

The Advanced LIGO gravitational-wave detectors offer a unique perspective on this problem. Advanced LIGO is a pair of Michelson interferometers, each with 4 km long Fabry–Pérot arm cavities formed by 40 kg mirrors that hang on fused silica fibers (Fig. 1). The differential motion of each pair of arm cavity mirrors forms a mechanical oscillator with a reduced mass of 20 kg; the differential motion of each such oscillator in either arm, sensed by the Michelson interferometer, forms a mechanical oscillator of effective mass $m = 10$ kg that is the object of our attention. The oscillator follows the pendulum-like motion of the suspended mirror at a frequency $\Omega_0 \approx 2\pi \cdot 0.43$ Hz; gravitational stress dilution is expected to realize a quality factor of $Q_0 \approx 10^8$ [11]. Its displacement fluctuates due to the presence of $n_{\text{th}}[\Omega_0] \approx 10^{13}$ phonons. The interferometer resonantly transduces the differential arm motion into optical power fluctuations at the anti-symmetric port, which is sensed by homodyne detection; during ordinary operation, these fluctuations encode the gravitational-wave signals. In this state, the homodyne photocurrent fluctuations bear the apparent displacement $\delta x_{\text{obs}} = \delta x + \delta x_{\text{imp}}$; here δx is the physical motion of the differential arm, which contains the displacement of the oscillator, and δx_{imp} is the measurement imprecision. The imprecision noise, depicted in Fig. 1B, is $2 \cdot 10^{-20}$ m/$\sqrt{\text{Hz}}$ around 100–200 Hz and is largely quantum shot noise — suppressed by ~ 3 dB by injection of squeezed light [12], and shaped by the response of the signal recycling cavity — with a secondary contribution from mechanical dissipation in the mirror coatings [13]. This sensitivity is equivalent to $n_{\text{imp}} \equiv S_x^{\text{imp}}/2S_x^{\text{zp}} \approx 3.5 \cdot 10^{-13}$ phonons for a 10 kg oscillator at ~ 150 Hz — a record low number (Ref. [9] demonstrates $n_{\text{imp}} \approx 10^{-7}$) tantamount to resolv-
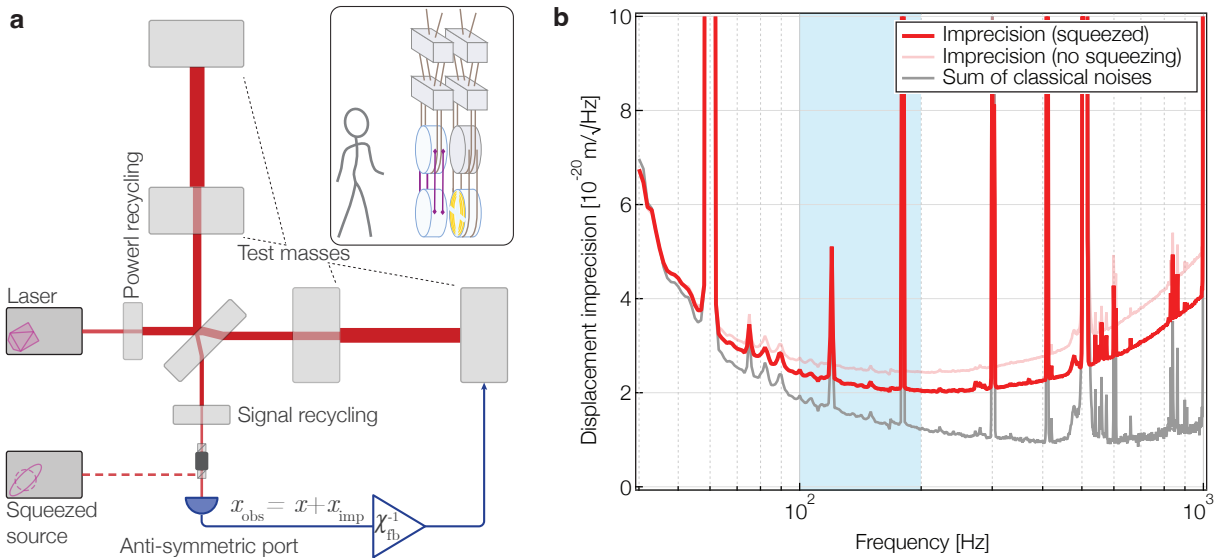
_____

* vivishek@mit.edu

FIG. 1. Advanced LIGO interferometer. (A) Laser light is split and recombined at a beam-splitter, forming a Michelson interferometer. Its response is shaped by the Fabry–Pérot cavities in the arms and the signal-recycling mirror. The power-recycling mirror and injection of squeezed light enhances the sensitivity. Inset shows the suspension system of each of the four 40 kg mirrors: the final mass on the forward chain is the 40 kg mirror, suspended on fused silica wires (purple) featuring a quality factor $Q \approx 8 \cdot 10^7$; they can be displaced by electrostatic forces due to voltages applied on electrodes (yellow) etched onto the reaction mass suspended behind it; average human sketched for scale. (B) The displacement sensitivity (red) of the interferometer is $2 \cdot 10^{-20}$ m/$\sqrt{\text{Hz}}$ at 100–200 Hz, where it is largely shot-noise (light red), suppressed by about 3 dB from injection of squeezed vacuum (red), and a combination of extraneous technical noises (gray). Blue band shows the frequency interval in which the pendulum mode is trapped and cooled.

ing the zero-point motion of the oscillator with ~ 125 dB signal to squeezed-shot-noise ratio, and comparable to the requirement to feedback cool the oscillator to its ground state ($n_{\text{imp}} \sim 1/2 n_{\text{th}}$, for a viscously-damped oscillator [14]).

In order to take advantage of this precision, we actively stiffen the pendulum mode by synthesizing a force proportional to the observed displacement (i.e. $\propto \Omega_{\text{fb}}^2 \delta x_{\text{obs}}$) and in-phase with the motion δx, trapping the pendulum mode as an oscillator around $\Omega_{\text{fb}} \approx 2\pi \cdot 148$ Hz. Two additional sources of decoherence plague this scheme. First, such measurement precision comes at the expense of additional quantum back-action on the pendulum mode: radiation pressure shot noise from the 200 kW intracavity power and the anti-squeezed intracavity field produces motion [15] equivalent to about $n_{\text{ba}}[\Omega_0] \approx 1.0 \cdot 10^{12}$ phonons. However, as long as the measurement record resolves the quantum back-action at a rate comparable to the thermal decoherence, active feedback can suppress it [9, 14, 16]. Secondly, the feedback of amplified imprecision noise leads to an additional "feedback back-action", $n_{\text{fb}} \approx Q_0^2 (\Omega_{\text{fb}}/\Omega_0)^4 n_{\text{imp}}$ (see Supplementary Information), which increases with the trap frequency. However, this is partially compensated by the $\Omega_{\text{fb}}/\Omega_0 \approx 300$ fold reduction in both the thermal occupation and decay rate of the trapped oscillator due to structural damping [5].

To trap and damp the oscillator, we adjust the feedback control so that $\delta F_{\text{fb}} = \chi_{\text{fb}}^{-1} \delta x_{\text{obs}}$, with a feedback

filter, $\chi_{\text{fb}}^{-1} \propto \Omega_{\text{fb}}^2 + i\Omega\Gamma_{\text{fb}}$, between 100–200 Hz. This is implemented by careful shaping of the control loop that is otherwise used to stabilize the interferometer at its linear operating point. The feedback force is applied on the mirror electrostatically: gold electrodes on the reaction mass (Fig. 1A) are held at a 400 V bias, whose fringing field polarizes the dielectric test mass; control voltages added on interleaved electrodes produce a proportional force (extraneous force noise produces $\ll 1$ phonon of excess occupation on average, see Supplementary Information). The overall feedback gain is adjusted so that the system's effective susceptibility takes the form, $\chi_{\text{eff}}[\Omega] \propto (-\Omega^2 + \Omega_{\text{eff}}^2 + i\Omega\Gamma_{\text{eff}}[\Omega])^{-1}/m$, of that of an oscillator with frequency $\Omega_{\text{eff}} = \sqrt{\Omega_0^2 + \Omega_{\text{fb}}^2} \approx \Omega_{\text{fb}} \approx 2\pi \cdot 148$ Hz. Delays in the feedback loop limit the trap frequency and cause the oscillator to be intrinsically "cold-damped". In particular, the phase response of the notch filters used to prevent excitation of the violin modes of the suspension (at 500 Hz and harmonics, featuring quality factors $\gtrsim 10^9$) in conjunction with the feedback filter leaves the interferometer's length control system with a phase margin of 1° for a trap frequency of 148 Hz. Physical delay in the loop also cold-damps the trapped oscillator to a quality factor of ≈ 50 (Fig. 2B red trace; see SI for further details). The oscillator is damped further by modifying the imaginary part of the feedback filter. Fig. 2A shows the effective susceptibilities of the trapped and damped oscillator so realized. The largest damping rate, corresponding to
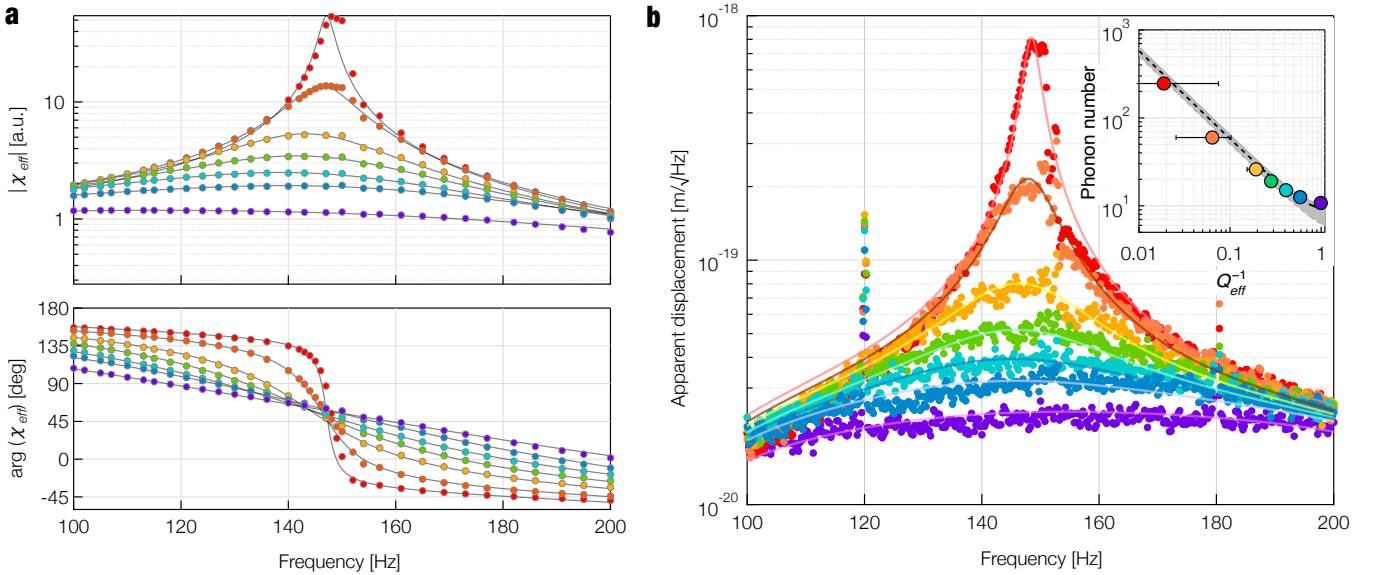
FIG. 2. Trapping and cooling of a 10 kg oscillator to 10 quanta. (A) Effective susceptibility of the oscillator for each setting of the damping filter, measured by exciting the feedback loop at each frequency and demodulating its response at the same frequency. The lines show fits to a model of the susceptibility of a damped harmonic oscillator with an additional delay, i.e. $\chi_{\text{eff}}[\Omega]e^{i\Omega\tau}$; fits to the phase response produce $\tau = 0.9$ ms. (B) Displacement spectrum of the oscillator as the damping is increased. Solid lines show fits to a model of the observed spectrum S_x^{obs} (see text for details) where the effective susceptibility is determined by the response measurements in panel (A), and only the frequency-dependent imprecision noise and force noise are variable. Inset shows the inferred average phonon occupation for each of the curves in the main panel, as a function of the damping quality factor; also shown is a model (black dashed) with model uncertainties (gray band). (The disagreement between the simple model and data — both the transfer functions and spectra — around 150–155 Hz arises from a coupling between the motion of the pendulum and the upper intermediate mass of the suspension [17].)

a quality factor of ≈ 1, is limited by the gain margin ($\approx 10^{-3}$) of the control loop. Around the trap frequency (100–200 Hz), additional force noise on the oscillator due to feedback is dominated by sub-quantum fluctuations of the squeezed imprecision noise.

The calibrated in-loop signal, depicted in Fig. 2B, shows the apparent displacement fluctuations of the trapped and damped oscillator (δx_{obs}). This can be understood using a simple model (see Supplementary Information), $\delta x_{\text{obs}} = \chi_{\text{eff}}(\delta F_{\text{th}} + \delta F_{\text{ba}} - \chi_{\text{fb}}^{-1}\delta x_{\text{imp}}) + \delta x_{\text{imp}}$. It describes the oscillator — with intrinsic susceptibility χ_0 — whose displacement responds via the feedback-modified effective susceptibility $\chi_{\text{eff}} = (\chi_0^{-1} + \chi_{\text{fb}}^{-1})^{-1}$, to three forces: a frequency-dependent structural thermal force (δF_{th}), a white quantum measurement back-action force (δF_{ba}), and an additional force noise ($\propto \chi_{\text{fb}}^{-1}\delta x_{\text{imp}}$) due to feedback of imprecision noise through the feedback filter; and riding on the imprecision noise (δx_{imp}). The spectra of the observed displacement S_x^{obs} predicted by this model are shown as the solid lines in Fig. 2B. In the model, the effective susceptibility is fully determined by the response measurements shown in Fig. 2A, independent of the frequency-dependent force noise and imprecision noise. The latter, determined self-consistently amongst the displacement noise in Fig. 2B, shows a variation between the different feedback settings of less than 1%, consistent with expected drift in the Advanced LIGO interferometer

over the ~ 2 hr timescale over which the experiment was performed. Several sources of uncertainty are accounted for in this process. Calibration of the displacement spectra contributes $\approx 2\%$ uncertainty [17]. Uncertainties in the effective susceptibility χ_{eff} — from fits to Fig. 2A — are at the 1% level, limited by the 1 s averaging used per point in measurements of the response (see Supplementary Information). The dominant uncertainty is in the fits to the displacement spectra of Fig. 2B using the model for S_x^{obs}: the frequency-dependence of the imprecision noise and structurally damped thermal force noise produce a $\approx 5\%$ variation between the various spectra in Fig. 2B.

The effective phonon occupation (n_{eff}) of the cooled oscillator can be defined through, $\hbar\Omega_{\text{eff}}(n_{\text{eff}} + \frac{1}{2}) = \langle p^2/(2m) + m\Omega_{\text{eff}}^2 x^2/2\rangle$, where x (p) is the physical displacement (momentum) of the oscillator at the trap frequency. Assuming the displacement and momentum to be zero-mean, their second moments can be estimated as the integral of their spectral densities. In principle, two factors complicate this procedure: at lower frequencies, structural damping renders the displacement variance singular [5], while at higher frequencies, feedback back-action precludes a finite momentum variance [29]. In practice, the feedback filter $\chi_{\text{fb}}^{-1} \propto \Omega_{\text{fb}}^2 + i\Omega\Gamma_{\text{fb}}$ is established around 100–200 Hz in an envelope that falls-off at least as Ω^{-2} (at frequencies below 10 Hz, the interferometer's length
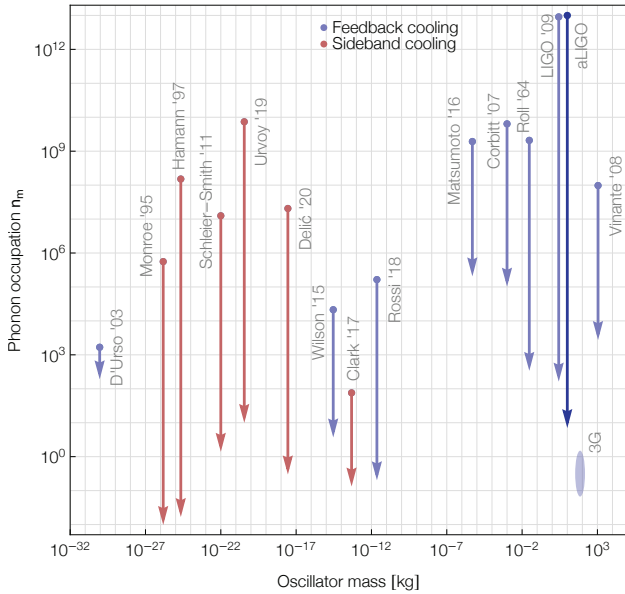
FIG. 3. A selection of oscillator cooling experiments [9, 10, 14, 18–28]. The initial occupations mentioned are those of the relevant oscillator mode as defined by the natural trap frequency, at its ambient temperature. For atomic physics experiments, this is usually at room temperature in a harmonic electromagnetic trap; whereas for most solid-state mechanical oscillators, it is the harmonic mode defined by the Hookean restoring force of its elastic suspension, and typically at cryogenic temperatures (the exception is the recent work from Delić et al. [10] which demonstrated cavity-cooling of an electromagnetically trapped nano-particle to its ground state). Our result ("aLIGO") sets a new record in the macroscopic mass range, reaching 10.8 ± 0.8 phonons. Experiments with future gravitational-wave interferometers ("3G") will achieve occupations below 1.

control loop picks up again), which regulates both these problems. In this fashion, within 100–200 Hz, the trapped oscillator approximately satisfies the equipartition principle, and so an effective phonon occupation can be assigned using the physical displacement spectrum:

$$n_{\text{eff}} \approx \int \frac{S_x[\Omega]}{2x_{\text{zp}}^2} \frac{d\Omega}{2\pi}.$$

Note that the 100 Hz frequency band in which the oscillator is established is much larger than the expected decoherence rate of the trapped oscillator, $(n_{\text{th}}[\Omega_{\text{eff}}] + n_{\text{ba}} + n_{\text{fb}}[\Omega_{\text{eff}}])\Gamma_0[\Omega_{\text{eff}}] \approx 2\pi \cdot 10\,\text{Hz}$. We evaluate the integral using the physical displacement spectrum reconstructed from fits to the observed displacement. The minimum phonon occupation of the 10 kg oscillator, corresponding to the purple trace in Fig. 2B, is thus inferred to be 10.8 ± 0.8; this is equivalent to an effective mode temperature of 77 nK. This demonstration sets a new record for the quantum state purity ($\approx 10\%$ ground state fidelity) for an object of such large mass (see Fig. 3).

The preparation of massive objects progressively nearer their ground state opens the door for more sophisticated demonstrations and applications of macroscopic quantum phenomena and quantum metrology. The most intriguing possibility, however, harnesses the ready susceptibility of kg-scale masses to gravitational forces; with this work, it becomes possible to prepare them in near-quantum states. This hints at the tantalizing prospect of studying gravitational decoherence on massive quantum systems.

[1] F. Karolyhazy, Il Nuovo Cimento A **42**, 390 (1966).
[2] L. Diósi, Physical Review A **40**, 1165 (1989).
[3] R. Penrose, General Relativity and Gravitation **28**, 581 (1996).
[4] A. Bassi, A. Großardt, and H. Ulbricht, Classical and Quantum Gravity **34**, 193002 (2017).
[5] P. R. Saulson, Physical Review D **42**, 2437 (1990).
[6] J. Chan, T. P. M. Alegre, A. H. Safavi-Naeini, J. T. Hill, A. Krause, S. Gröblacher, M. Aspelmeyer, and O. Painter, Nature **478**, 89 (2011).
[7] J. D. Teufel, T. Donner, D. Li, J. W. Harlow, M. S. Allman, K. Cicak, A. J. Sirois, J. D. Whittaker, K. W. Lehnert, and R. W. Simmonds, Nature **475**, 359 (2011).
[8] R. Peterson, T. Purdy, N. Kampel, R. Andrews, P.-L. Yu, K. Lehnert, and C. Regal, Physical Review Letters **116**, 063601 (2016).
[9] M. Rossi, D. Mason, J. Chen, Y. Tsaturyan, and A. Schliesser, Nature **563**, 53 (2018).
[10] U. Delić, M. Reisenbauer, K. Dare, D. Grass, V. Vuletić, N. Kiesel, and M. Aspelmeyer, Science **367**, 892 (2020).
[11] A. V. Cumming, A. S. Bell, L. Barsotti, M. A. Barton, G. Cagnoli, D. Cook, L. Cunningham, M. Evans, G. D. Hammond, G. M. Harry, A. Heptonstall, J. Hough, R. Jones, R. Kumar, R. Mittleman, N. A. Robertson, S. Rowan, B. Shapiro, K. A. Strain, K Tokmakov, C. Torrie, and A. A. v. Veggel, Classical and Quantum Gravity **29**, 035003 (2012).
[12] M. Tse, H. Yu, N. Kijbunchoo, A. Fernandez-Galiana, P. Dupej, L. Barsotti, C. Blair, D. Brown, S. Dwyer, A. Effler, M. Evans, P. Fritschel, V. Frolov, A. Green, G. Mansell, F. Matichard, N. Mavalvala, D. McClelland, L. McCuller, T. McRae, J. Miller, A. Mullavey, E. Oelker, I. Phinney, D. Sigg, B. Slagmolen, T. Vo, R. Ward, C. Whittle, R. Abbott, C. Adams, R. Adhikari, A. Ananyeva, S. Appert, K. Arai, J. Areeda, Y. Asali, S. Aston, C. Austin, A. Baer, M. Ball, S. Ballmer, S. Banagiri, D. Barker, J. Bartlett, B. Berger, J. Betzwieser, D. Bhattacharjee, G. Billingsley, S. Biscans, R. Blair, N. Bode, P. Booker, R. Bork, A. Bramley, A. Brooks, A. Buikema, C. Cahillane, K. Cannon, X. Chen, A. Ciobanu, F. Clara, S. Cooper, K. Corley, S. Countryman, P. Covas, D. Coyne, L. Datrier,

D. Davis, C. Di Fronzo, J. Driggers, T. Etzel, T. Evans, J. Feicht, P. Fulda, M. Fyffe, J. Giaime, K. Giardina, P. Godwin, E. Goetz, S. Gras, C. Gray, R. Gray, A. Gupta, E. Gustafson, R. Gustafson, J. Hanks, J. Hanson, T. Hardwick, R. Hasskew, M. Heintze, A. Helmling-Cornell, N. Holland, J. Jones, S. Kandhasamy, S. Karki, M. Kasprzack, K. Kawabe, P. King, J. Kissel, R. Kumar, M. Landry, B. Lane, B. Lantz, M. Laxen, Y. Lecoeuche, J. Leviton, J. Liu, M. Lormand, A. Lundgren, R. Macas, M. MacInnis, D. Macleod, S. Márka, Z. Márka, D. Martynov, K. Mason, T. Massinger, R. McCarthy, S. McCormick, J. McIver, G. Mendell, K. Merfeld, E. Merilh, F. Meylahn, T. Mistry, R. Mittleman, G. Moreno, C. Mow-Lowry, S. Mozzon, T. Nelson, P. Nguyen, L. Nuttall, J. Oberling, R. Oram, B. O'Reilly, C. Osthelder, D. Ottaway, H. Overmier, J. Palamos, W. Parker, E. Payne, A. Pele, C. Perez, M. Pirello, H. Radkins, K. Ramirez, J. Richardson, K. Riles, N. Robertson, J. Rollins, C. Romel, J. Romie, M. Ross, K. Ryan, T. Sadecki, E. Sanchez, L. Sanchez, T. Saravanan, R. Savage, D. Schaetzl, R. Schnabel, R. Schofield, E. Schwartz, D. Sellers, T. Shaffer, J. Smith, S. Soni, B. Sorazu, A. Spencer, K. Strain, L. Sun, M. Szczepańczyk, M. Thomas, P. Thomas, K. Thorne, K. Toland, C. Torrie, G. Traylor, A. Urban, G. Vajente, G. Valdes, D. Vander-Hyde, P. Veitch, K. Venkateswara, G. Venugopalan, A. Viets, C. Vorvick, M. Wade, J. Warner, B. Weaver, R. Weiss, B. Willke, C. Wipf, L. Xiao, H. Yamamoto, M. Yap, H. Yu, L. Zhang, M. Zucker, and J. Zweizig, Physical Review Letters **123**, 231107 (2019).

[13] A. Buikema, C. Cahillane, G. Mansell, C. Blair, R. Abbott, C. Adams, R. Adhikari, A. Ananyeva, S. Appert, K. Arai, J. Areeda, Y. Asali, S. Aston, C. Austin, A. Baer, M. Ball, S. Ballmer, S. Banagiri, D. Barker, L. Barsotti, J. Bartlett, B. Berger, J. Betzwieser, D. Bhattacharjee, G. Billingsley, S. Biscans, R. Blair, N. Bode, P. Booker, R. Bork, A. Bramley, A. Brooks, D. Brown, K. Cannon, X. Chen, A. Ciobanu, F. Clara, S. Cooper, K. Corley, S. Countryman, P. Covas, D. Coyne, L. Datrier, D. Davis, C. Di Fronzo, K. Dooley, J. Driggers, P. Dupej, S. Dwyer, A. Effler, T. Etzel, M. Evans, T. Evans, J. Feicht, A. Fernandez-Galiana, P. Fritschel, V. Frolov, P. Fulda, M. Fyffe, J. Giaime, K. Giardina, P. Godwin, E. Goetz, S. Gras, C. Gray, R. Gray, A. Green, E. Gustafson, R. Gustafson, J. Hanks, J. Hanson, T. Hardwick, R. Hasskew, M. Heintze, A. Helmling-Cornell, N. Holland, J. Jones, S. Kandhasamy, S. Karki, M. Kasprzack, K. Kawabe, N. Kijbunchoo, P. King, J. Kissel, R. Kumar, M. Landry, B. Lane, B. Lantz, M. Laxen, Y. Lecoeuche, J. Leviton, J. Liu, M. Lormand, A. Lundgren, R. Macas, M. MacInnis, D. Macleod, S. Márka, Z. Márka, D. Martynov, K. Mason, T. Massinger, F. Matichard, N. Mavalvala, R. McCarthy, D. McClelland, S. McCormick, L. McCuller, J. McIver, T. McRae, G. Mendell, K. Merfeld, E. Merilh, F. Meylahn, T. Mistry, R. Mittleman, G. Moreno, C. Mow-Lowry, S. Mozzon, A. Mullavey, T. Nelson, P. Nguyen, L. Nuttall, J. Oberling, R. J. Oram, B. O'Reilly, C. Osthelder, D. Ottaway, H. Overmier, J. Palamos, W. Parker, E. Payne, A. Pele, R. Penhorwood, C. Perez, M. Pirello, H. Radkins, K. Ramirez, J. Richardson, K. Riles, N. Robertson, J. Rollins, C. Romel, J. Romie, M. Ross, K. Ryan, T. Sadecki, E. Sanchez, L. Sanchez, T. Saravanan, R. Savage, D. Schaetzl, R. Schnabel, R. Schofield, E. Schwartz, D. Sellers, T. Shaf-

fer, D. Sigg, B. Slagmolen, J. Smith, S. Soni, B. Sorazu, A. Spencer, K. Strain, L. Sun, M. Szczepańczyk, M. Thomas, P. Thomas, K. Thorne, K. Toland, C. Torrie, G. Traylor, M. Tse, A. Urban, G. Vajente, G. Valdes, D. Vander-Hyde, P. Veitch, K. Venkateswara, G. Venugopalan, A. Viets, T. Vo, C. Vorvick, M. Wade, R. Ward, J. Warner, B. Weaver, R. Weiss, C. Whittle, B. Willke, C. Wipf, L. Xiao, H. Yamamoto, H. Yu, H. Yu, L. Zhang, M. Zucker, and J. Zweizig, Physical Review D **102**, 062003 (2020).

[14] D. J. Wilson, V. Sudhir, N. Piro, R. Schilling, A. Ghadimi, and T. J. Kippenberg, Nature **524**, 325 (2015).

[15] H. Yu, L. McCuller, M. Tse, N. Kijbunchoo, L. Barsotti, N. Mavalvala, J. Betzwieser, C. D. Blair, S. E. Dwyer, A. Effler, M. Evans, A. Fernandez-Galiana, P. Fritschel, V. V. Frolov, F. Matichard, D. E. McClelland, T. McRae, A. Mullavey, D. Sigg, B. J. J. Slagmolen, C. Whittle, A. Buikema, Y. Chen, T. R. Corbitt, R. Schnabel, R. Abbott, C. Adams, R. X. Adhikari, A. Ananyeva, S. Appert, K. Arai, J. S. Areeda, Y. Asali, S. M. Aston, C. Austin, A. M. Baer, M. Ball, S. W. Ballmer, S. Banagiri, D. Barker, J. Bartlett, B. K. Berger, D. Bhattacharjee, G. Billingsley, S. Biscans, R. M. Blair, N. Bode, P. Booker, R. Bork, A. Bramley, A. F. Brooks, D. D. Brown, C. Cahillane, K. C. Cannon, X. Chen, A. A. Ciobanu, F. Clara, S. J. Cooper, K. R. Corley, S. T. Countryman, P. B. Covas, D. C. Coyne, L. E. H. Datrier, D. Davis, C. Di Fronzo, K. L. Dooley, J. C. Driggers, P. Dupej, T. Etzel, T. M. Evans, J. Feicht, P. Fulda, M. Fyffe, J. A. Giaime, K. D. Giardina, P. Godwin, E. Goetz, S. Gras, C. Gray, R. Gray, A. C. Green, A. Gupta, E. K. Gustafson, R. Gustafson, J. Hanks, J. Hanson, T. Hardwick, R. K. Hasskew, M. C. Heintze, A. F. Helmling-Cornell, N. A. Holland, J. D. Jones, S. Kandhasamy, S. Karki, M. Kasprzack, K. Kawabe, P. J. King, J. S. Kissel, R. Kumar, M. Landry, B. B. Lane, B. Lantz, M. Laxen, Y. K. Lecoeuche, J. Leviton, J. Liu, M. Lormand, A. P. Lundgren, R. Macas, M. MacInnis, D. M. Macleod, G. L. Mansell, S. Márka, Z. Márka, D. V. Martynov, K. Mason, T. J. Massinger, R. McCarthy, S. McCormick, J. McIver, G. Mendell, K. Merfeld, E. L. Merilh, F. Meylahn, T. Mistry, R. Mittleman, G. Moreno, C. M. Mow-Lowry, S. Mozzon, T. J. N. Nelson, P. Nguyen, L. K. Nuttall, J. Oberling, R. J. Oram, C. Osthelder, D. J. Ottaway, H. Overmier, J. R. Palamos, W. Parker, E. Payne, A. Pele, C. J. Perez, M. Pirello, H. Radkins, K. E. Ramirez, J. W. Richardson, K. Riles, N. A. Robertson, J. G. Rollins, C. L. Romel, J. H. Romie, M. P. Ross, K. Ryan, T. Sadecki, E. J. Sanchez, L. E. Sanchez, T. R. Saravanan, R. L. Savage, D. Schaetzl, R. M. S. Schofield, E. Schwartz, D. Sellers, T. Shaffer, J. R. Smith, S. Soni, B. Sorazu, A. P. Spencer, K. A. Strain, L. Sun, M. J. Szczepańczyk, M. Thomas, P. Thomas, K. A. Thorne, K. Toland, C. I. Torrie, G. Traylor, A. L. Urban, G. Vajente, G. Valdes, D. C. Vander-Hyde, P. J. Veitch, K. Venkateswara, G. Venugopalan, A. D. Viets, T. Vo, C. Vorvick, M. Wade, R. L. Ward, J. Warner, B. Weaver, R. Weiss, B. Willke, C. C. Wipf, L. Xiao, H. Yamamoto, H. Yu, L. Zhang, M. E. Zucker, and J. Zweizig, Nature **583**, 43 (2020).

[16] V. Sudhir, D. Wilson, R. Schilling, H. Schütz, S. Fedorov, A. Ghadimi, A. Nunnenkamp, and T. Kippenberg, Physical Review X **7**, 011001 (2017).

[17] L. Sun, E. Goetz, J. Kissel, J. Betzwieser, S. Karki, A. Vi-

ets, M. Wade, D. Bhattacharjee, V. Bossilkov, P. B. Covas, L. E. H. Datrier, R. Gray, S. Kandhasamy, Y. Lecoeuche, G. Mendell, T. Mistry, E. Payne, R. Savage, A. J. Weinstein, S. Aston, A. Buikema, C. Cahillane, J. C. Driggers, S. Dwyer, R. Kumar, and A. L. Urban, Classical and Quantum Gravity **37**, 225008 (2020).

[18] B. D'Urso, B. Odom, and G. Gabrielse, Physical Review Letters **90**, 043001 (2003).

[19] C. Monroe, D. M. Meekhof, B. E. King, S. R. Jefferts, W. M. Itano, D. J. Wineland, and P. Gould, Phys. Rev. Lett. **75**, 4011 (1995).

[20] S. E. Hamann, D. L. Haycock, G. Klose, P. H. Pax, I. H. Deutsch, and P. S. Jessen, Phys. Rev. Lett. **80**, 4149 (1998).

[21] M. H. Schleier-Smith, I. D. Leroux, H. Zhang, M. A. Van Camp, and V. Vuletić, Phys. Rev. Lett. **107**, 143005 (2011).

[22] A. Urvoy, Z. Vendeiro, J. Ramette, A. Adiyatullin, and V. Vuletić, Phys. Rev. Lett. **122**, 203202 (2019).

[23] J. B. Clark, F. Lecocq, R. W. Simmonds, J. Aumentado, and J. D. Teufel, Nature **541**, 191 (2017).

[24] N. Matsumoto, K. Komori, S. Ito, Y. Michimura, and Y. Aso, Phys. Rev. A **94**, 033822 (2016).

[25] T. Corbitt, C. Wipf, T. Bodiya, D. Ottaway, D. Sigg, N. Smith, S. Whitcomb, and N. Mavalvala, Phys. Rev. Lett. **99**, 160801 (2007).

[26] P. G. Roll, R. Krotkov, and R. H. Dicke, Annals of Physics **26**, 442 (1964).

[27] B. Abbott et al., New Journal of Physics **11**, 073032 (2009).

[28] A. Vinante, M. Bignotto, M. Bonaldi, M. Cerdonio, L. Conti, P. Falferi, N. Liguori, S. Longo, R. Mezzena, A. Ortolan, G. A. Prodi, F. Salemi, L. Taffarello, G. Vedovato, S. Vitale, and J.-P. Zendri, Physical Review Letters **101**, 033601 (2008).

[29] D. Vitali, S. Mancini, L. Ribichini, and P. Tombesi, Journal of the Optical Society of America B **20**, 1054 (2003).

[30] B. P. Abbott et al., Physical Review D **95**, 062003 (2017).

[31] A. Buikema, *High-Power Operation of Interferometric Gravitational-Wave Detectors*, Ph.D. thesis, MIT (2019).

[32] J. Bendat and A. Piersol, *Random Data: Analysis and Measurement Procedures*, 4th ed., Wiley Series in Probability and Statistics (Wiley, 2011).

[33] P. T. Boggs, C. H. Spiegelman, J. R. Donaldson, and R. B. Schnabel, Journal of Econometrics **38**, 169 (1988).

Appendix A: Model of measurement and feedback

The displacement of the oscillator (δx) responds to a sum of thermal, back-action, and feedback forces:

$$\chi_0^{-1}\delta x = \delta F_{\text{th}} + \delta F_{\text{ba}} + F_{\text{fb}}. \tag{A1}$$

Here, the susceptibility of the oscillator $\chi_0^{-1}[\Omega] = m(-\Omega^2 + \Omega_0^2 + i\Omega\Gamma_0[\Omega])$ is well approximated by the test mass pendulum mode at frequency $\Omega_0 \approx 2\pi \cdot 0.43\,\text{Hz}$, which is structurally damped, so that its damping rate is frequency dependent: $\Gamma_0[\Omega] = (\Omega_0/Q_0)(\Omega_0/\Omega)$, with a quality factor $Q_0 \approx 10^8$.

The thermal force (δF_{th}) is characterized by its spectral density,

$$S_F^{\text{th}}[\Omega] = 4\hbar\left(n_{\text{th}}[\Omega] + \tfrac{1}{2}\right)\text{Im}\,\chi_0^{-1}[\Omega], \tag{A2}$$

where $n_{\text{th}}[\Omega] \approx k_B T/(\hbar\Omega) \approx 9 \cdot 10^{12}(\Omega_0/\Omega)$ is the average thermal phonon occupation. The back-action force (δF_{ba}), arising from radiation pressure quantum fluctuations, is characterized by

$$S_F^{\text{ba}}[\Omega] = \frac{16\hbar\mathcal{F}}{\lambda c}P_{\text{cav}}e^{2r_{\text{asqz}}}, \tag{A3}$$

where $P_{\text{cav}} \approx 200\,\text{kW}$ is the mean arm cavity power at wavelength $\lambda = 1064\,\text{nm}$, $\mathcal{F} \approx 45$ is the effective finesse of the signal-recycled arm cavities, and r_{asqz} quantifies the increase in quantum fluctuations of the intracavity optical amplitude due to antisqueezing due to the phase-squeezed vacuum injected at the interferometer's dark port; here $10\log_{10}e^{2r_{\text{asqz}}} = (8 \pm 1)\,\text{dB}$ [15]. The back-action force can be quantified in terms of an average phonon occupation n_{ba} via $S_F^{\text{ba}} \equiv 4\hbar n_{\text{ba}}\,\text{Im}\,\chi_0^{-1}[\Omega_0]$, which gives $n_{\text{ba}} \approx 1.0 \cdot 10^{12}$.
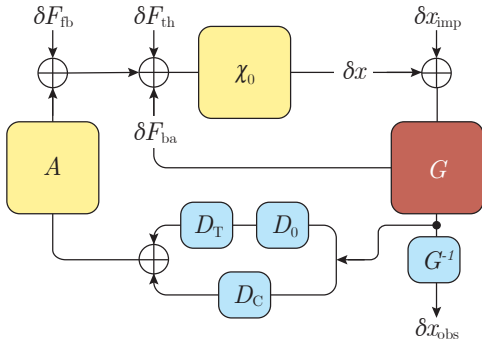
FIG. 4. Schematic of the physical system consisting of the intrinsic mechanical response χ_0, the interferometer's sensing function G, the digital filters $D_{0,\mathrm{T,C}}$, and the actuation A; G^{-1} denotes the digital filter used to reconstruct the apparent displacement. The feedback is subject to fluctuations arising from actuator force noise δF_{fb}, thermal noise δF_{th}, back-action noise δF_{ba} and imprecision noise δx_{imp}.

The feedback force F_{fb} is based on a linear estimate of the oscillator's position,

$$\delta x_{\mathrm{est}} \equiv G(\delta x + \delta x_{\mathrm{imp}}); \qquad (\mathrm{A4})$$

here, δx_{imp} is the displacement imprecision (due to sensing noise), and G is the sensing function of the interferometer. Such an estimate is obtained only when the interferometer is stabilized at its linear operating point, achieved by a feedback loop that forces the test mass (modeled by the actuation function A) based on a filtered (by D_0) record of the error signal x_{est}. We create an additional feedback path consisting of a digital filter D_{T} in series with D_0 to produce the trap, and a parallel path consisting of the digital filter D_{C} to cold-damp the trapped oscillator. The combined feedback force thus exerted is

$$
\begin{aligned}
F_{\mathrm{fb}} &= A(D_0 D_{\mathrm{T}} + D_{\mathrm{C}})\delta x_{\mathrm{est}} + \delta F_{\mathrm{fb}} \\
&\equiv -\chi_{\mathrm{fb}}^{-1}(\delta x + \delta x_{\mathrm{imp}}) + \delta F_{\mathrm{fb}};
\end{aligned}
\qquad (\mathrm{A5})
$$

here, δF_{fb} models extraneous force fluctuations due to the actuator. Solving for δx between Eqs. (A1) and (A5) gives the physical displacement fluctuations,

$$\delta x = \chi_{\mathrm{eff}}\left(\delta F_{\mathrm{tot}} - \chi_{\mathrm{fb}}^{-1}\delta x_{\mathrm{imp}}\right); \qquad (\mathrm{A6})$$

here, $\chi_{\mathrm{eff}} \equiv (\chi_0^{-1} + \chi_{\mathrm{fb}}^{-1})^{-1}$ is the effective susceptibility of the oscillator, and $\delta F_{\mathrm{tot}} \equiv \delta F_{\mathrm{th}} + \delta F_{\mathrm{ba}} + \delta F_{\mathrm{fb}}$ is the total force noise.

The oscillator can be trapped and cooled by synthesizing an effective susceptibility of the form,

$$\chi_{\mathrm{eff}}^{-1} = m(-\Omega^2 + \Omega_{\mathrm{eff}}^2 + i\Omega\Gamma_{\mathrm{eff}}). \qquad (\mathrm{A7})$$

We are able to do this by careful design of the effective loop filter χ_{fb}^{-1}, which is switched on in a sequence that both traps the oscillator, and keeps the interferometer unconditionally stable.

What we observe is the apparent displacement δx_{obs} inferred using an estimate for the inverse sensing function

G^{-1} (that forms part of LIGO's calibration pipeline [30]). That is, $\delta x_{\mathrm{obs}} \equiv G^{-1}\delta x_{\mathrm{est}} \approx \delta x + \delta x_{\mathrm{imp}}$; amplitude uncertainty in this estimate is at the 2% level [17]. Using the known expression for the physical displacement in Eq. (A6), the apparent displacement is,

$$\delta x_{\mathrm{obs}} = \chi_{\mathrm{eff}}\left(\delta F_{\mathrm{tot}} + \chi_0^{-1}\delta x_{\mathrm{imp}}\right). \qquad (\mathrm{A8})$$

This model produces the spectrum of the observed signal,

$$
\begin{aligned}
S_x^{\mathrm{obs}}[\Omega] =& \frac{S_F^{\mathrm{tot}}[\Omega]/m^2}{(\Omega_{\mathrm{eff}}^2 - \Omega^2)^2 + (\Omega\Gamma_{\mathrm{eff}})^2} \\
&+ \frac{(\Omega_0^2 - \Omega^2)^2 + (\Omega\Gamma_0[\Omega])^2}{(\Omega_{\mathrm{eff}}^2 - \Omega^2)^2 + (\Omega\Gamma_{\mathrm{eff}})^2} S_x^{\mathrm{imp}}[\Omega],
\end{aligned}
\qquad (\mathrm{A9})
$$

that is used to fit the data in Fig. 2B in the main text. However the apparent motion — since it contains correlations impressed by the feedback of imprecision — cannot be directly compared to the spectrum of a physical oscillator that is damped.

The spectrum of the physical motion of the oscillator (δx in Eq. (A6)),

$$
\begin{aligned}
S_x[\Omega] =& \frac{S_F^{\mathrm{tot}}[\Omega]/m^2}{(\Omega_{\mathrm{eff}}^2 - \Omega^2)^2 + (\Omega\Gamma_{\mathrm{eff}})^2} \\
&+ \frac{\Omega_{\mathrm{fb}}^4 + (\Omega\Gamma_{\mathrm{fb}})^2}{(\Omega_{\mathrm{eff}}^2 - \Omega^2)^2 + (\Omega\Gamma_{\mathrm{eff}})^2} S_x^{\mathrm{imp}}[\Omega],
\end{aligned}
\qquad (\mathrm{A10})
$$

can be directly compared against that of an oscillator trapped at frequency Ω_{eff}, and featuring a damped linewidth Γ_{eff}. Writing $x = x_{\mathrm{zp}}(b + b^\dagger)$ for the position of such an oscillator, with zero-point motion $x_{\mathrm{zp}} = \sqrt{\hbar/2m\Omega_{\mathrm{eff}}}$ and creation operator b, presumed to exist in a thermal state, we use the identities,

$$\mathrm{Var}[x] = 2x_{\mathrm{zp}}^2\left(\langle b^\dagger b\rangle + \tfrac{1}{2}\right) \qquad (\mathrm{A11})$$

$$\mathrm{Var}[x] = \int S_x[\Omega]\,\frac{\mathrm{d}\Omega}{2\pi}, \qquad (\mathrm{A12})$$

to assign an effective phonon number $n_{\mathrm{eff}} \equiv \langle b^\dagger b\rangle$:

$$n_{\mathrm{eff}} + \tfrac{1}{2} = \int \frac{S_x[\Omega]}{2x_{\mathrm{zp}}^2}\,\frac{\mathrm{d}\Omega}{2\pi}. \qquad (\mathrm{A13})$$

Here, the integral is understood to be evaluated in the frequency interval where the oscillator susceptibility is realized.

When the imprecision noise is white (i.e. $S_x^{\mathrm{imp}}[\Omega] \approx S_x^{\mathrm{imp}}[\Omega_{\mathrm{eff}}]$), and the frequency-dependence of the structurally-damped thermal phonon number can be neglected (i.e. $n_{\mathrm{th}}[\Omega] \approx n_{\mathrm{th}}[\Omega_{\mathrm{eff}}]$) — both inapplicable to the current experiment, but useful to develop intuition — the phonon occupation can be explicitly evaluated as,

$$
\begin{aligned}
n_{\mathrm{eff}} + \frac{1}{2} \approx & \left(n_{\mathrm{tot}}[\Omega_{\mathrm{eff}}] + \left(\frac{\Omega_{\mathrm{eff}}}{\Gamma_0[\Omega_{\mathrm{eff}}]}\right)^2 n_{\mathrm{imp}} + \frac{1}{2}\right)\frac{\Gamma_0[\Omega_{\mathrm{eff}}]}{\Gamma_{\mathrm{eff}}[\Omega_{\mathrm{eff}}]} \\
& + n_{\mathrm{imp}}\frac{\Gamma_{\mathrm{eff}}[\Omega_{\mathrm{eff}}]}{\Gamma_0[\Omega_{\mathrm{eff}}]},
\end{aligned}
$$
$$(\mathrm{A14})$$

where the factor in the parentheses in the first line is the total initial occupation, consisting of the sum of thermal and back-action quanta ($n_{\text{tot}} = n_{\text{th}} + n_{\text{ba}}$), and an additional contribution $(\Omega_{\text{eff}}/\Gamma_0)^2 n_{\text{imp}}$ due to fluctuations in the trap from feedback of imprecision noise due to the active spring. Here, $n_{\text{imp}} \equiv S_x^{\text{imp}}[\Omega_{\text{eff}}]/2S_x^{\text{zp}}[\Omega_{\text{eff}}]$, is the phonon-equivalent imprecision ($S_x^{\text{zp}}[\Omega_{\text{eff}}] = 8x_{\text{zp}}^2/\Gamma_0[\Omega_{\text{eff}}]$ is the peak zero-point spectrum of the trapped oscillator).

1. Effect of actuator force noise

It has been documented that the electrostatic drive (ESD) that is used to actuate the test masses produces excess force noise that arises from a combination of charging effects and driver voltage noise [31]. In the context of feedback cooling the test mass, this force (termed δF_{fb} in Eq. (A6)) acts as an excess thermal force that heats the trapped oscillator, resulting in additional phonons (n_{fb}) that add to the thermal occupation. From Ref. [31], it can be inferred that

$$\sqrt{S_F^{\text{fb}}} \approx (4 \cdot 10^{-18} \, \text{N}/\sqrt{\text{Hz}}) \left(\frac{10 \, \text{Hz}}{f} \right).$$

(By comparison, the typical actuation strength used to keep the interferometer locked is $\sim 10^{-6} \, \text{N}/\sqrt{\text{Hz}}$ at 10 Hz.) An extraneous phonon occupation $n_{\text{fb,ex}}$ can be associated with this force noise via, $S_F^{\text{fb}} \approx 4\hbar m \Gamma_0 \Omega_{\text{eff}} n_{\text{fb,ex}}$. Assuming the oscillator is trapped at $\Omega_{\text{eff}} \approx 2\pi \cdot 148$ Hz, the equivalent phonon occupation from excess ESD noise is, $n_{\text{fb,ex}} \lesssim 10^{-3}$.

2. Effect of filter delay

If the feedback is implemented with an overall delay τ — for example arising from delays in the computation of the digital filter — the trapping and cooling filter is modified to

$$\chi_{\text{fb}}^{-1} e^{i\Omega\tau} = m(\Omega_{\text{fb}}^2 + i\Omega\Gamma_{\text{fb}})e^{i\Omega\tau}$$
$$\approx m[\Omega_{\text{fb}}^2(1 - \tau\Gamma_{\text{fb}}) + i\Omega(\Gamma_{\text{fb}} + \tau\Omega_{\text{fb}}^2)],$$

where in going to the second line, we assume that the delay is small compared to the characteristic frequency at which it occurs, i.e. $\Omega\tau \ll 1$. Thus, even in the absence of active damping (i.e. $\Gamma_{\text{fb}} = 0$), delay in the loop manifests as damping $\tau\Omega_{\text{fb}}^2$. This serves to stabilize the trapped oscillator.

Delay in other parts of the loop manifest as an overall phase factor in the closed-loop gain, $\chi_{\text{eff}} e^{i\Omega\tau}$. Fits to the phase response of the closed-loop gain in the main text resolve this overall phase shift at the level of ≈ 0.9 ms, consistent with expected delays in the loop.

Appendix B: Data analysis

1. Uncertainty in transfer function fits

The standard deviation in the transfer function estimate $\hat{G}$ derived from signals with coherence C over N averages is given by [32]

$$\sigma_{\hat{G}} = \sqrt{\frac{(1-C)}{2CN}}\hat{G}. \tag{B1}$$

Similarly, the coherence estimate $\hat{C}$ has standard deviation

$$\sigma_{\hat{C}} = \sqrt{\frac{2C}{N}}(1-C). \tag{B2}$$

Even assuming a worst-case true coherence C within this range, most of the uncertainty in our data arises from the 1 s average duration and corresponding 1 Hz bin width.

We fit to a time-delayed resonator model,

$$\chi_{\text{eff}} \sim \frac{1}{\Omega_0^2 - \Omega^2 + i\Omega_0\Omega/Q} e^{i(\phi - \Omega t)}, \tag{B3}$$

and propagate these uncertainties using orthogonal distance regression [33].